Optimization of temperature characteristics of a transportable ^{87}Rb atomic fountain clock

Xinwen Wang (王新文)[1,2], Kangkang Liu (刘亢亢)[1], Henan Cheng (程鹤楠)[1], Wei Ren (任 伟)[1], Jingfeng Xiang (项静峰)[1], Jingwei Ji (吉经纬)[1], Xiangkai Peng (彭向凯)[1,2], Zhen Zhang (张 镇)[1], Jianbo Zhao (赵剑波)[1], Meifeng Ye (叶美凤)[1], Lin Li (李 琳)[1], Tang Li (李 唐)[1], Bin Wang (汪 斌)[1], Qiuzhi Qu (屈求智)[1], Liang Liu (刘 亮)[1,*], and Desheng Lü (吕德胜)[1,2,]**

[1]*Key Laboratory of Quantum Optics, Shanghai Institute of Optics and Fine Mechanics, Chinese Academy of Sciences, Shanghai 201800, China*

[2]*College of Materials Science and Opto-Electronic Technology, University of Chinese Academy of Sciences, Beijing 100049, China*

**Corresponding author: liang.liu@siom.ac.cn; **corresponding author: dslv@siom.ac.cn*

Received March 29, 2019; accepted May 17, 2019; posted online July 15, 2019

A high-performance transportable fountain clock is attractive for use in laboratories with high-precision time-frequency measurement requirements. This Letter reports the improvement of the stability of a transportable rubidium-87 fountain clock because of an optimization of temperature characteristics. This clock integrates its physical packaging, optical benches, microwave frequency synthesizers, and electronic controls onto an easily movable wheeled plate. Two optical benches with a high-vibration resistance are realized in this work. No additional adjustment is required after moving them several times. The Allan deviation of the fountain clock frequency was measured by comparing it with that of the hydrogen maser. The fountain clock got a short-term stability of 2.3×10^{-13} at 1 s and long-term stability on the order of 10^{-16} at 100,000 s.

OCIS codes: 020.3320, 120.3940, 270.2500, 270.5570.
doi: 10.3788/COL201917.080201.

Since the first demonstration of a cesium fountain atomic clock in 1991[1] and its use as a frequency standard in 1995[2], the accuracy of frequency standards based on these technologies has reached $2-4 \times 10^{-16}$[3–6], which can thus provide the most accurate realization of the international system of units (SI) second and define the accuracy of international atomic time (TAI)[7]. A number of groups worldwide are now realizing an accurate SI second locally using cesium fountain clocks in the laboratory[3–6,8]. Frequency transfer via an optical fiber link between laboratories has become popular because of the high performance available[9–12]. However, a transportable clock offers considerable flexibility for point-to-point frequency comparisons. While transportable lattice optical clocks have been demonstrated in relativistic geodesy applications with an uncertainty of 2.7×10^{-17}[13], a compact and user-friendly fountain clock remains interesting for many laboratories with high-precision time-frequency measurement requirements. For example, the mobile cesium clock from SYRTE[14] can operate in a gravity and a microgravity environment. In gravity, the mobile cesium fountain can deliver a primary reference signal with an accuracy of 6.9×10^{-16}[3]. In the $\sim 10^{-2}$ g gravity environment produced by jet plane parabolic flights it gets a resonance linewidth of 7 Hz. When compared with cesium atoms, rubidium-87 atoms have a smaller cold collision frequency shift[15–18] and the cooling laser operating at 780 nm is relatively easy to obtain, so rubidium fountain clocks are easier to develop and are more reliable. Four rubidium fountains have been in operation at the US Naval Observatory for over five years, demonstrating their long-term stability[19]. This Letter introduces preliminary results for a transportable rubidium fountain atomic clock. We expect to be able to use this high-precision clock to perform frequency calibration services for atomic clocks located in different areas.

Figure 1 shows a cutaway and picture of the rubidium fountain clock apparatus. The entire system is set on a

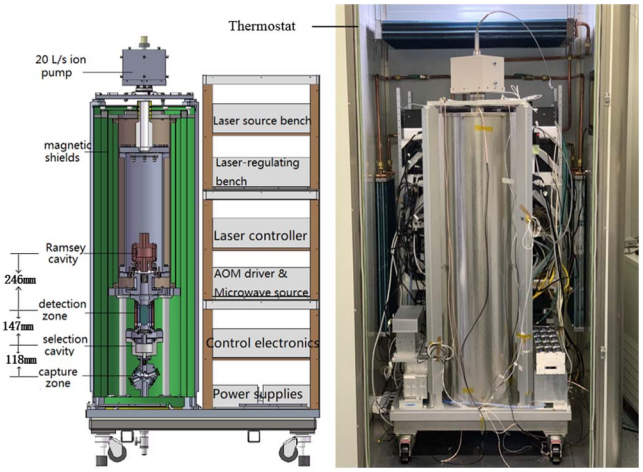

Fig. 1. Cutaway and picture of the transportable fountain clock assembly. The size and weight of the clock are about 96 cm × 76 cm × 180 cm and 350 kg, respectively.

metal table with four wheels, which is convenient for transport. The size and weight of the clock are about 96 cm × 76 cm × 180 cm and 350 kg, respectively. The physical package is on the left side of the table, where the vacuum chamber is enclosed within three layers of magnetic shielding. From bottom to top, the vacuum chamber is composed of four parts: the cooling zone, the state selection and detection zone, the main chamber, and the ion pump. In the cooling zone, background thermal ^{87}Rb atoms are captured and cooled in a three-dimensional magneto-optical trap (MOT), and are then launched vertically via the moving molasses method in a (1,1,1) geometry[4]. During the upward motion of the atoms, only those in the sub state are stimulated by the state selection cavity, while all atoms in other magnetic states are removed from the laser beam. Inside the main vacuum chamber, a Ramsey cavity operates in TE011 mode with a resonant frequency of 6.834 GHz. The cavity is made from oxygen-free high thermal conductivity copper (OFHC) with a loaded quality factor of 4000. Microwave power is fed into the cavity via two apertures at opposing positions within the cavity wall. This microwave coupling method is beneficial in reducing the phase difference of the microwave field within the cavity[20]. After the atoms interact twice (i.e., on the way up and then down again) with the resonant microwave field in the Ramsey cavity, the relative populations of the two ground hyperfine states change depending on the frequency detuning of the microwave field from the atomic transition resonance. Finally, the changes in the populations of the two ground states are measured in the detection zone during the downward movement of the atoms. From the changes in their populations, we can defer detuning of the microwave frequency and lock it to the atomic transition frequency.

The vacuum pressure inside the chamber is always lower than 10^{-7} Pa, and this pressure is maintained using a 20 L/s ion pump (Agilent) and four getter pumps (ST171, SAES Getters Co., Ltd.) that are located on top of the main chamber. All vacuum chamber walls are made from titanium (TC4). In addition to the three outer layers of magnetic shielding, another shielding layer encloses the main vacuum chamber to ensure maximum attenuation of the ambient magnetic field inside the chamber. Between the chamber and the innermost shield, a wound solenoid generates a bias magnetic field (C-field) of approximately 100 nT that is used as a quantization axis for the atoms.

The optical system consists of a laser source bench and a laser-regulating bench. There are two external cavity laser diodes (ECDLs) and a tapered amplifier (TA) on the laser source bench, as shown in Fig. 2(a). The system will produce a cooling laser beam and a repumping laser beam, which are respectively locked onto the '23' and '12' crossover resonances of the saturated absorption of the ^{87}Rb D2 line. An automatic frequency stabilization system that can sweep the laser frequency automatically and lock the target saturated absorption peak is used on this bench. Approximately 600 mW from the cooling laser, amplified using the TA, and 30 mW from the repumping laser, are

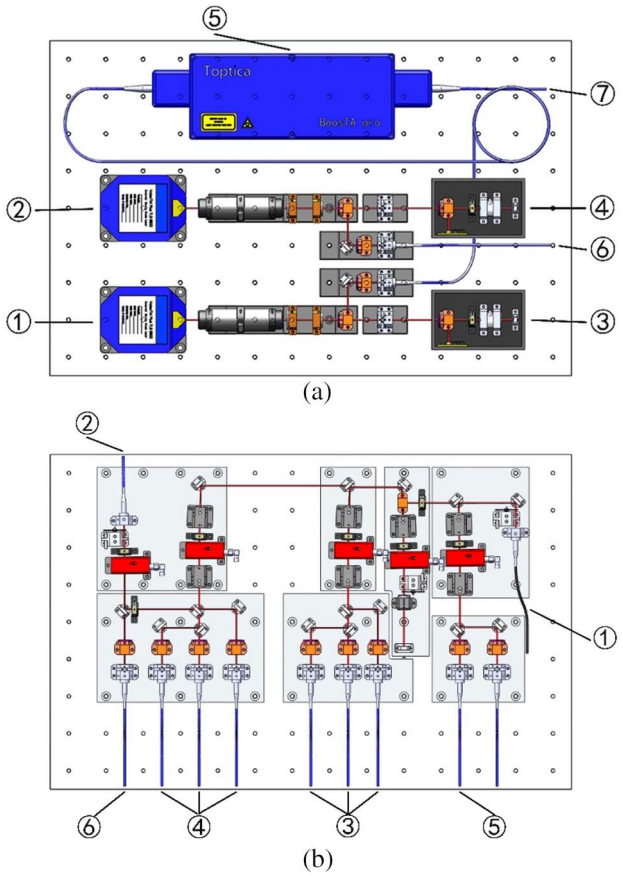

Fig. 2. Model diagrams of the optical benches. (a) The laser source bench with ECDL and TA, which is used to produce and amplify the cooling laser and the repumping laser. ①, ②: ECDLs; ③, ④: the saturation absorption modules; ⑤: TA; ⑥: the repumping laser output; ⑦: cooling laser output. (b) The laser-regulating bench divides and combines the cooling laser or repumping laser. ①: cooling laser input; ②: repumping laser input; ③: upward cooling laser output; ④: downward cooling laser output; ⑤: detection laser output; ⑥ repumping laser output.

coupled into two independent single-mode polarization-maintaining fibers that are connected to another laser-regulating bench, which is shown in Fig. 2(b). The cooling laser beam is then divided into seven beams, where one is used as the detection laser and the other six beams are used as cooling lasers. The repumping laser beam is divided into two beams, where one is used for repumping atoms in the detection region and the other beam is combined into the cooling laser for repumping atoms in the atom collection region. Acousto-optic modulators and mechano-optical switches are used in the light passage to control the laser frequency and power. A programmable sequencer controls the laser frequencies and power during the various phases of the fountain cycle (i.e., molasses capture, atom launching, sub-Doppler cooling, and detection)[21,22].

None of the components on the benches require further adjustment after the high-precision mounting and adjustment procedure because they are carefully designed to be insensitive to vibration. The modular and antivibration

design of the optical bench is convenient for adjustment and transfer[23]. The benches can easily be removed from the shelves, if necessary.

We have developed a microwave synthesizer to generate the required microwave clock frequency from the local 5 MHz reference oscillation. A two-step phase-locked loop (PLL) architecture was used in this frequency synthesis chain[24]. The output microwave signal benefits from both the ultra-high close-up spectral purity of the reference oscillator and the low phase noise level of the PLL at frequencies in a range that is far from the carrier. The output microwave power can be adjusted over the range from −20.5 to −81.75 dBm, and the resulting signals are fed to both the state selection cavity and the Ramsey cavity.

In our fountain clock cycle, approximately 10^8 atoms are initially captured within 1 s using the MOT[25,26]; at this phase, the frequency of the cooling laser is detuned from the optical cooling transition by approximately −18 MHz. The magnetic field of the MOT is then switched off and the trapped atoms expand within the optical molasses for 10 ms; at the end of this phase, the detuning of the cooling laser sweeps to −48 MHz in 2 ms for the pre-cooling stage. In the third phase, the laser detuning is redrawn to −12 MHz and the atoms are launched via the moving molasses method by tuning the three up and down cooling lasers in the opposite direction. When the atoms are first launched, with an initial speed of 4 m/s, the frequency detuning of the moving optical molasses is increased to −48 MHz for 500 μs; subsequently, the light field amplitude is switched off adiabatically within another 500 μs. Using the time-of-flight method, the temperature of the launched atoms was measured to be approximately 7 μK, although this temperature is currently limited by the magnetic field of the cooling fiber connector's ferrule, which is both ferric and close to the center of the MOT.

After state selection and two Ramsey interactions, the number of atoms that reach the detection region is estimated to be approximately 4.5×10^5. The Ramsey fringes were acquired by scanning the microwave frequency of the Ramsey cavity, as shown in Fig. 3. The linewidth of the central fringes is approximately 1.02 Hz.

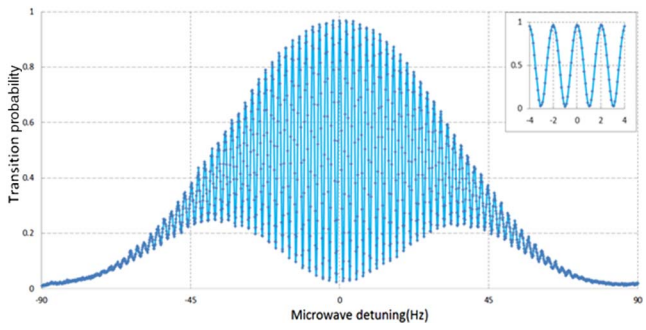

Fig. 3. Ramsey pattern obtained by scanning the microwave frequency of the Ramsey cavity using 0.1 Hz steps. The inset curve is the transition probability versus detuning of the microwave signal by several Hz; the linewidth of the central fringe is approximately 1.02 Hz.

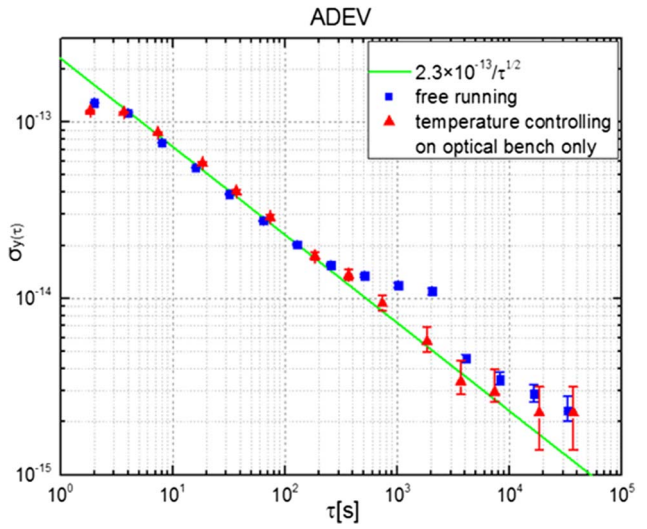

Fig. 4. Short- and medium-term stabilities of the fountain clock with MOT on. The square dots are the Allan deviations obtained with the clock operating in our laboratory where the temperature fluctuation is about ±1.5°C. The triangle dots are the Allan deviations obtained with temperature control of the optical bench. The solid line is a fitted curve corresponding to a white frequency noise of $2.3 \times 10^{-13}\tau^{-1/2}$.

Figure 4 shows the Allan deviation of the frequency, which was measured by comparing the frequency of the fountain with that of a hydrogen maser (T4 Science). The stability of the clock corresponding to white frequency noise is $2.3 \times 10^{-13}\tau^{-1/2}$, shown as a solid line in Fig. 4. In the medium term, the frequency stability described by the square dots shows a drift when the averaging time is 500–4000 s. According to the records of temperature on the optical benches, laser power, and the number of detected atoms, as shown in Fig. 5, we find that the number of atoms and laser power were both correlated with fluctuations in the temperature of the optical benches, and the drift of frequency in the medium term

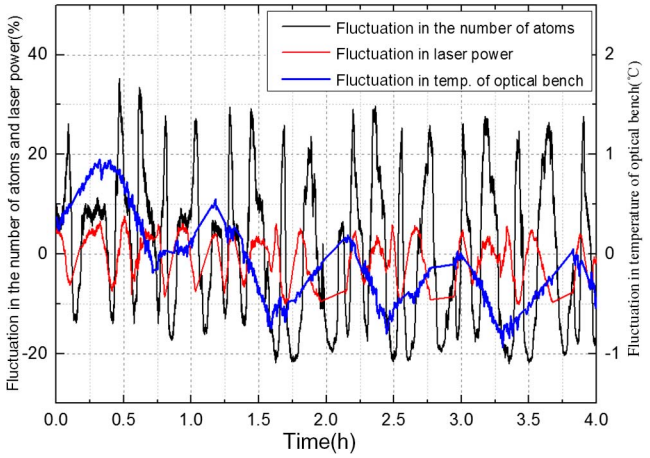

Fig. 5. Fluctuation in the number of atoms, laser power, and temperature of the optical bench before temperature controlling of the optical bench.

was quite consistent with the fluctuation period of the number of atoms. After controlling the temperature of the two optical benches, the fluctuation of the optical bench temperatures was reduced to ±0.2°C, and the fluctuation in the number of atoms was reduced to less than 10%. The medium-term Allan deviation of the fountain frequency was thus improved, as shown by the triangle dots in Fig. 4. However, when the average measurement time τ exceeds 10,000 s, the Allan deviation drifts again. Better temperature control may be necessary for the entire fountain atomic clock.

We customized a 200 cm × 120 cm × 100 cm enclosed thermostat whose temperature is controlled by a water cooler with three cooling plates circulating constant temperature water. In addition, in order to reduce the heating effect of the pulsed MOT coils' current, we use the optical molasses method to capture the cold atoms by shutting down the MOT coils' current. The fountain clock was put into the thermostat, as shown in Fig. 1. After the fountain clock ran for a few days inside, the thermostat temperature distribution reached equilibrium with a fluctuation less than 0.1°C while fluctuation in the temperature of the optical benches was only within 0.01°C. The fluctuation in the number of atoms was reduced to less than 7%, as shown in Fig. 6, which shows that the fluctuation in temperature of optical benches does not contribute to the number of atoms, but the air temperature in the thermostat does. Because the detection of the laser power is not available to us in the thermostat at present, we speculate that the air temperature may affect the power or polarization of the laser in the optical fiber, resulting in a fluctuation in the number of atoms.

After stable operation of the fountain clock, we got the Allan deviation of the frequency, as the square dots show in Fig. 7. The short-term stability described by the solid line got up to $4 \times 10^{-13}\tau^{-1/2}$ because the number of atoms captured by molasses is about one tenth of that obtained by MOT. However, when the averaging time goes up to 100,000 s, the stability reaches up to the order of 10^{-16} and continues going down. This shows a good improvement on the long-term stability when the entire clock is temperature controlled in the thermostat.

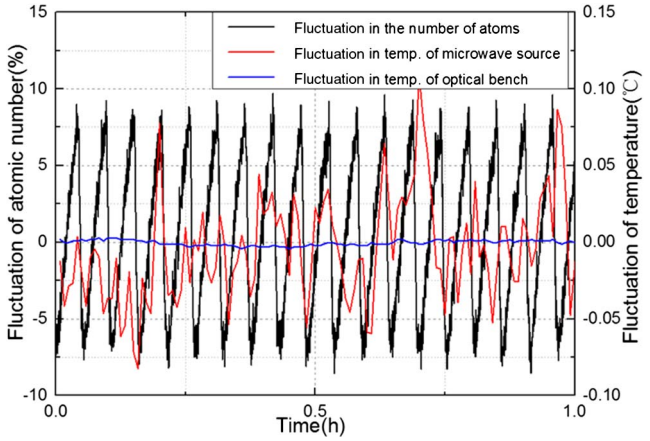

Fig. 6. Fluctuation in the number of atoms, temperature of the microwave source, and the optical benches when the fountain clock was operated in the thermostat.

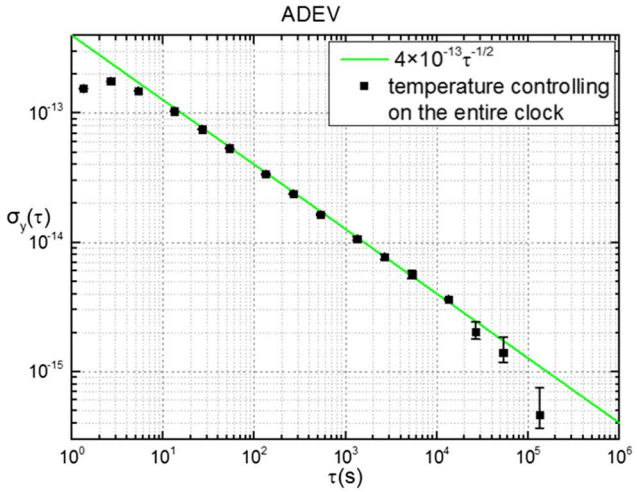

Fig. 7. Allan deviation of the fountain clock frequency with MOT off when it was put into the thermostat. The solid line is the fitting curve of short-term stability. After the averaging time exceeds 100,000 s, the long-term stability reaches the order of 10^{-16} and continues going down.

In conclusion, we developed a transportable ^{87}Rb fountain atomic clock in which the physical package, the optical benches, the microwave frequency synthesizers, and the electronic controls were integrated onto an easily movable wheeled plate. Using the captured atoms at approximately 7 μK, we obtained a clock transition spectrum with a linewidth of approximately 1.02 Hz. The short-term stability of this fountain clock was demonstrated to be 2.3×10^{-13} at 1 s. The fractional stability of the frequency reached the order of 10^{-16} and will continue going down. A good optimization of the long-term stability is accomplished by controlling the ambient temperature fluctuations of the entire clock in the enclosed thermostat. Our next work is to evaluate the uncertainty of the rubidium fountain using a frequency comparison with the primary cesium fountain clock.

This work was supported by the Ministry of Science and Technology of China (No. 2013YQ09094304) and the National Natural Science Foundation of China (No. 11034008).

References

1. A. Clairon, C. Salomon, S. Guellati, and W. D. Phillips, Europhys. Lett. **16**, 16165 (1991).
2. C. Vian, P. Rosenbusch, H. Marion, S. Bize, L. Cacciapuoti, S. Zhang, M. Abgrall, D. Chambon, I. Maksimovic, P. Laurent, G. Santarelli, A. Clairon, A. Luiten, M. Tobar, and C. Salomon, IEEE Instrum. Meas. **54**, 833 (2005).
3. J. Guéna, M. Abgrall, D. Rovera, P. Laurent, B. Chupin, M. Lours, G. Santarelli, P. Rosenbusch, M. E. Tobar, R. Li, K. Gibble, A. Clairon, and S. Bize, IEEE Trans. Ultrason. Eng. **59**, 391 (2012).
4. V. Gerginov, N. Nemitz, S. Weyers, R. Schröder, D. Griebsch, and R. Wynands, Metrologia **47**, 65 (2009).

5. Y. Ovchinnikov and G. Marra, Metrologia **48**, 87 (2011).
6. F. Levi, D. Calonico, C. E. Calosso, A. Godone, S. Micalizio, and G. A. Costanzo, Metrologia **51**, 270 (2014).
7. T. E. Parker, Rev. Sci. Instrum. **83**, 021102 (2012)
8. F. Fang, M. Li, P. Lin, W. Chen, N. Liu, Y. Lin, P. Wang, K. Liu, R. Suo, and T. Li, Metrologia **52**, 454 (2015).
9. C. Lisdat, G. Grosche, N. Quintin, C. Shi, S. M. F. Raupach, C. Grebing, D. Nicolodi, F. Stefani, A. Al-Masoudi, S. Dorscher, S. Hafner, J.-L. Robyr, N. Chiodo, S. Bilicki, E. Bookjans, A. Koczwara, S. Koke, A. Kuhl, F. Wiotte, F. Meynadier, E. Camisard, M. Lours, T. Legero, H. Schnatz, U. Sterr, H. Denker, C. Chardonnet, Y. Le Cop, G. Santarelli, A. Amy-Klein, R. Le Targat, J. Lodewyck, O. Lopez, and P.-E. Pottie, Nat. Commun. **7**, 12443 (2016)
10. W. Chen, Q. Liu, N. Cheng, D. Xu, F. Yang, Y. Gui, and H. Cai, IEEE Photonics J. **7**, 7901609 (2015).
11. Y. Bai, B. Wang, C. Gao, J. Miao, X. Zhu, and L. Wang, Chin. Opt. Lett. **13**, 061201 (2015).
12. F. Chen, K. Zhao, X. Zhou, T. Liu, and S. Zhang, Acta Phys. Sin. **66**, 200701 (2017).
13. J. Grotti, S. Koller, S. Vogt, S. Häfner, U. Sterr, C. Lisdat, H. Denker, C. Voigt, L. Timmen, A. Rolland, N. Baynes, F. S. Margolis, M. Zampaolo, P. Thoumany, M. Pizzocaro, B. Rauf, F. Bregolin, A. Tampellini, P. Barbier, M. Zucco, A. Costanzo, C. Clivati, F. Levi, and D. Calonico, Nat. Phys. **14**, 437 (2018).
14. P. Laurent, P. Lemonde, E. Simon, G. Santarelli, A. Clairon, N. Dimarcp, P. Petit, C. Audoin, and C. Salomon, Eurp. Phys. J. D **3**, 201 (1998).
15. S. J. Kokkelmans, B. J. Verhaar, K. Gibble, and D. J. Heinzen Phys. Rev. A **56**, R4389 (1997).
16. S. Bize, Y. Sortais, M. S. Santos, C. Mandache, A. Clairon, and C. Salomon, Europhys. Lett. **45**, 558 (1999).
17. G. Dong, J. Deng, J. Lin, S. Zhang, H. Lin, and Y. Wang, Chin. Opt. Lett. **15**, 040201 (2017).
18. R. Dong, J. Lin, R. Wei, W. Wang, F. Zou, Y. Du, T. Chen, and Y. Wang, Chin. Opt. Lett. **15**, 050201 (2017).
19. S. Peil, T. B. Swanson, J. Hanssen, and J. Taylor, Metrologia **54**, 247 (2017).
20. R. Li and K. Gibble, Metrologia **47**, 534 (2010).
21. L. Liu, D. S. Lü, W. B. Chen, T. Li, Q. Z. Qu, B. Wang, L. Li, W. Ren, Z. R. Dong, J. B. Zhao, W. B. Xia, X. Zhao, J. W. Ji, M. F. Ye, Y. G. Sun, Y. Y. Yao, D. Song, Z. G. Liang, S. J. Hu, D. H. Yu, X. Hou, W. Shi, H. G. Zang, J. F. Xiang, X. K. Peng, and Y. Z. Wang, Nat. Commun. **9**, 2760 (2018).
22. L. Li, Q. Qu, B. Wang, T. Li, J. Zhao, J. Ji, W. Ren, X. Zhao, M. Ye, Y. Yao, D. Lü, and L. Liu, Chin. Phys. Lett. **33**, 063201 (2016).
23. Q. Qu, W. Xia, B. Wang, D. Lü, J. Zhao, M. Ye, W. Ren, J. Xiang, and L. Liu, Acta Opt. Sin. **35**, 0602003 (2015).
24. T. Li, J. Huang, Q. Qu, B. Wang, L. Li, W. Ren, W. Shi, J. B. Zhao, X. Zhao, J. W. Ji, M. F. Ye, Y. Y. Yao, D. S. Lü, Y. Z. Wang, W. B. Chen, and L. Liu, Rev. Sci. Instrum. **89**, 113115 (2018).
25. Q. Qu, B. Wang, D. Lü, J. Zhao, M. Ye, W. Ren, J. Xiang, and L. Liu, Chin. Opt. Lett. **13**, 061405 (2015).
26. B. Yang, J. Wang, and J. Wang, Chin. Opt. Lett. **14**, 040201 (2016).